A simple continuous-wave diffuse optical tomography system for parametric investigation of different tissue phantoms

M. PATACHIA
Department of Lasers, National Institute for Laser, Plasma and Radiation Physics, 409 Atomistilor St., PO Box MG-36, 077125 Magurele, Ilfov, Romania

Diffuse optical tomography (DOT) is a potential diagnostic tool for detecting abnormal growths in translucent soft tissues. Its principle is to use multiple movable light sources and detectors attached to the tissue surface to collect information on light attenuation, and to reconstruct the internal 3-D absorption and scattering distributions. The development of optical imaging techniques, like that of any other medical diagnostic modality, has relied upon appropriate phantoms whose physical properties and geometries are matched to those of human tissues. Measurements on phantoms are used to evaluate the performance of systems and to validate the imaging algorithms. Together with the reconstructions of the tissues structure, the calibration is the pivotal part of the data acquisition due to the variation in characteristics of each laser source, optical fibres, detectors, and optic elements. An accurate calibration is achieved in a homogeneous phantom. The work describes some methods to achieve homogeneous phantoms and how they are used to evaluate the performance of the system.

(Received November 14, 2012; accepted April 11, 2013)

Keywords: Laser Diode, Diffuse optical tomography, Optics fibre, Tissue phantom, Image reconstruction

1. Introduction

Started in 1929 as a simple transillumination, or diaphanography, the utilization of light to probe tissue has grew in the last years with the advent of new lasers, light detectors and fast computers and the development of the formalism for light propagation which demonstrates that light distribution in tissue can be well approximated with diffusion equation. Hence, the field of diffuse optical tomography (DOT) was born.

By DOT, the optical properties of the translucent soft tissues are reconstructed based on measurements of near-infrared (NIR) light at the boundary of the object. To obtain such data, DOT uses movable light sources and detectors attached to the surface of the target media. There are three main measurement schemes, namely:

- time domain (TD), where the illumination of the tissue with a very short light pulse (picosecond or femtosecond) enable the evaluation of the optical properties of the tissue from the detected broadened light pulse emerging the tissue surface;
- the frequency domain (FD), where the illumination of the tissue with a high frequency amplitude modulated light and the measurement of the amplitude and phase of the detected signal are used to derive the optical absorption (μ_a) and scattering (μ'_s) coefficients;
- continuous-wave (CW), where the measurement of the amplitude of the illumination signal at the boundary of the tissue enable the characterization of its optical properties by the total coefficient of absorption in the tissue.

This last method is used in our experiments, because it is more accessible from the technical point of view (low frequency modulation, high sensitive detectors, etc.) being at the same time the simplest and least expensive from the three schemes. The CW method provides also the fastest data collection.

The correct use of the CW method however needs a special effort to solve the non-uniqueness problem of the method which lacks the capability to separate absorption from scattering in the optical tomography (OT) image reconstruction. For this aim, the CW imaging needs preconditioning and regularization techniques and multispectral laser sources.

The need of multispectral light sources is demonstrated also by the spectral distribution of the absorption coefficient (Fig. 1) and the reduced scattering coefficient (Fig. 2) for the most important tissue components: oxy-hemoglobin, deoxy-hemoglobin, water, and lipids.

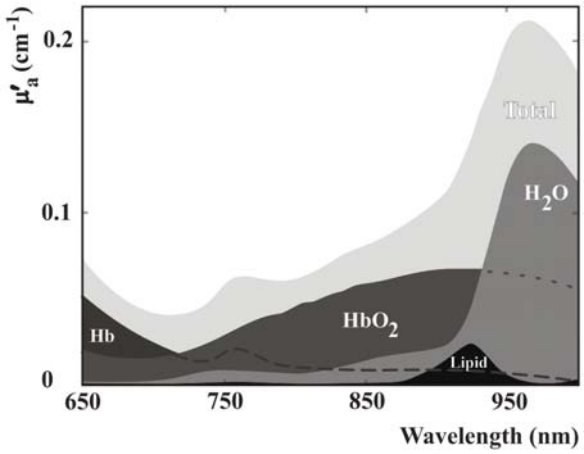

Fig.1 Absorption spectra of the primary tissue constituents.

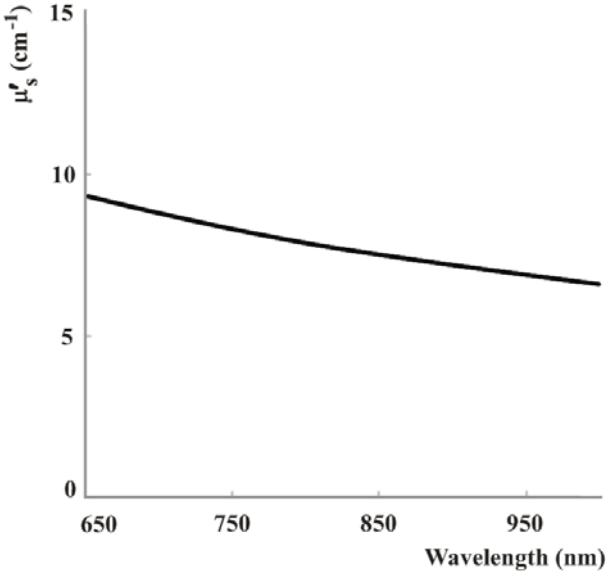

Fig. 2 Reduced scattering coefficient of tissue assuming to obey a simplified Mie-scattering law, i.e., $\mu'_s = A\lambda^{-b}$

2. Absorption and scattering in turbid media

Tissuesare a turbid media, characterized by many small random fluctuations in refractive index caused by the ultrastructure of the tissue, i.e., by cells and organelles. As a consequence of these refractive index fluctuations, light incident on tissue is deflected or scattered by these particles. Additionally, the tissues also contain chromophores, molecules that can absorb the incoming photons.

2.1 Absorption and the absorption coefficient

In an absorption event, energy is transferred from the radiation to the surrounding medium. The quantity which describes absorption in the medium is the absorption coefficient, μ_a, related to the number of absorption events per unit length.

2.2 Scattering, coefficient, scattering phase function and anisotropy factor

Scattering is a phenomenon in which the direction of the radiations changes randomly within the medium. The new radiation direction depends on the properties of the scatterer and the incoming direction of the radiation. The scattering properties of the medium are described by two quantities which are the scattering coefficient and the scattering phase function.

The scattering coefficient, μ_s, describes the probability of a particle to scatter after travelling a certain distance.

The scattering phase function, $P(\theta)$, describes the probability of a particle to scatter in a given direction by a particular scatterer.

The directionality of the scattered wavefront can be characterized by angles, θ and ψ, in a plane and perpendicular to it, respectively. In the literature, $P(\theta)$, is sometimes denoted $P(\hat{s},\hat{s}')$, i.e., the scattering phase function from direction, $\hat{s}$, into direction, $\hat{s}'$, or $P(\cos\theta)$ to denote the angular dependence. In the definition used here, θ is, by convention, only in the plane of the paper.

Since $P(\theta)$ is normalized, the component of the deflected path parallel to the incident path is $\cos\theta$, as it is drawn in dashed line (Fig. 3).

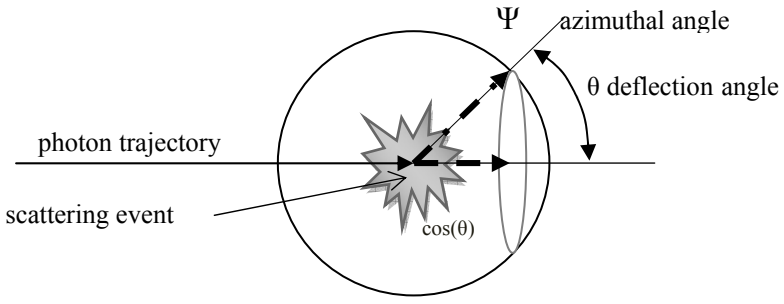

Fig. 3 Graphical description of a scattering event.

The deflection angle θ is formed between the paths of the scattered and the incident photon in the plane of the paper. Deflection is considered independent over azimuthal angle, ψ, in the plane perpendicular to the incident photon path.

This component is important, since it describes how isotropic or anisotropic the scattering is. Isotropic scattering is frequent when the particle is much smaller than the wavelength of light.

One can also define the anisotropy factor, g (also called asymmetry parameter or simply g-factor) as the expectation value of $\cos\theta$.

Mie theory provides an exact solution for the scattering and the anisotropy coefficients of perfect dielectric spheres of arbitrary size in a uniform background medium [1-3]. Using this theoretical framework, the reduced scattering spectra of bulk homogeneous samples can be approximately expressed by the following equation [1]:

$$\mu_s'(\lambda) = N_0(\pi a^2)Q_{scat}(m,a,\lambda)[1-g(m,a,\lambda)] \quad (1)$$

where λ is the wavelength, a is the diameter of the particle, m is the refractive index ratio from inside to outside the particles ($m = n_2/n_1$, where n_1 and n_2 are the refractive indexes outside and inside the particles, respectively), and $Q_{scat}(m,a,\lambda)$ is a dimensionless scattering efficiency factor calculated from an analytic series expansion, which is the solution of the scattered wave intensity by a sphere [1]. This expression is used to estimate the refraction and reflection from a spherical particle. The framework can be extended to approximate a multisized scattering particle medium by summing the scattering contributions over all particle sizes and adding an approximate normalized size distribution factor, $f(a)$, that compensates for the number of particles at each given size, in which case Eq. (1) becomes:

$$\mu_s'(\lambda) = N_0\sum_{i=1}^{p} f(a_i)(\pi a_i^2)Q_{scat}(m,a_i,\lambda)[1-g(m,a_i,\lambda)] \quad (2)$$

This equation has implicit assumptions that the particle index changes are all the same, which is a limitation that should be recalled when it is applied in various problems. However, it is possible that index changes typically result only in changes of amplitude in μ'_s, rather than changes in the spectral features in the NIR regime. Thus, while the assumption of constant n is unfortunate, it still does enable an estimation of the particle size, given some *a priori* information about the $f(a_i)$ function, which describes the histogram of particle number density per unit particle size.

Since the reduced scattering spectra, $\mu'_s(\lambda)$, depends on the particle number density per unit particle size, $f(a_i)$, it is important to carefully analyze how these particular functions might impact the results of the study. Three histogram shapes have been examined, including: (1) a step function, (2) a normalized Gaussian function, and (3) an exponentially decaying function. Each is used with the same average particle size and the same total number density to determine differences in μ'_s caused by different histogram shape assumptions.

Rather than applying Mie scattering theory directly, a more empirical approach was first proposed by van Staveren *et al.* [4], who fit the scattering spectrum of intralipid. Many research teams have adopted this approach to characterize the spectrum of the reduced scattering coefficient observed in tissues. Its spectra are considered to satisfy a power law relationship.

Empirically, when there is a broad range of scattering particle sizes, this spectrum is described [5, 6] by a power law curve of the type:

$$\mu_s'(\lambda) = A\lambda^{-b} \quad (3)$$

where A and b are model parameters for scattering amplitude and scattering power, respectively. Equation (3) describes a smooth function with no oscillations in the spectrum, and conveniently restricts the fitting process to only two parameters.

A third quantity which affects light propagation within the medium is the refractive index, n. Changes in the refractive index between different materials can cause reflection and refraction effects at the interfaces between the materials. In most of the DOT applications, the refractive index is assumed to be constant within the medium.

In most of the tissues, light propagation is dominated by scattering. As a result of this, after traveling the length of a few millimeters, light propagation in tissues can be described as a diffusive process. Different tissue types have distinct scattering properties and, therefore, this distinction can be imaged [7, 8].

Because the scattering coefficient in biological materials is generally larger than the absorption coefficient, most of the interesting information is related to the absorption. Especially the absorption spectra of hemoglobin, water, and lipids are of great interest [9].

Aside from μ_s, g, and μ_a, there are some other parameters that can be used to describe turbid media. One of them is the total attenuation coefficient, μ_t [L^{-1}], which is defined as $\mu_t = \mu_s + \mu_a$. Because, in general, $\mu_s >> \mu_a$, one can make the approximation: $\mu_t \sim \mu_s$. The inverse of μ_t is called the mean free path, which is the average distance a photon travels between scattering or absorption events.

Near-infrared DOT has found its applications in imaging of thick tissues such as breast and brain, due to its unique capability of extracting tissue functional information [10]. Analogously, DOT could be used for imaging other tissues such as human joints and associated bones.

3. Tissue simulating phantoms for optical spectroscopy and DOT imaging

The key to matching tissue properties in phantoms is a comprehensive understanding of the physical and biochemical characteristics of tissue that influence its interaction with light [11].

For small scale (< 1 mm) applications, it is important to match the absorption coefficient, $\mu_a(\lambda)$, the scattering

coefficient, $\mu_s(\lambda)$, and the anisotropy coefficient, $g(\lambda)$, which is defined as the average cosine of the scattering angle, θ.

Over larger distances (more than 3 to 5 scattering lengths, a scattering length being defined as the reciprocal of the scattering coefficient, $1/\mu_s$), matching the reduced scattering coefficient, μ'_s, also called the transport scattering coefficient, defined as $\mu'_s = (1- g)\mu_s$ is all that is required [12].

This "reduced" approximation follows observations in neutral particle scattering that over multiple scattering event lengths. An anisotropic scattering process appears identical to an isotropic scattering process with a reduced value for the effective scattering coefficient. In many cases of thick tissue transmission, it is possible to get away with mimicking the effective attenuation coefficient of a tissue, defined in the wavelength range where diffusion theory is accurate as $\mu_{eff} =(3\mu_a\mu'_s)^{-1/2}$. This is possible because the steady-state attenuation in homogeneous media is affected in the same way by the same relative change in absorption or scattering. Over long distances, diffusive processes appear to be attenuated exponentially with this single coefficient, and only when boundaries or temporal signals are introduced there is a discernable separation of the effects of μ_a and μ'_s. If the goal is to mimic the tissue transmission, then matching coefficient, μ_{eff}, can often be sufficient, but in most tissue spectroscopy applications, where the goal is to separate $\mu_a(\lambda)$ and $\mu'_s(\lambda)$ to allow spectral fitting, the tissue must have representative values for both these parameters.

Optical spectroscopy, imaging, and therapy tissue phantoms must have the scattering and absorption properties that are characteristic of human tissues, and over the past few decades, many useful models have been created.

Matrix materials typically are water, gelatin, agar, polyester or epoxy and polyurethane resin, room-temperature vulcanizing (RTV) silicon, or polyvinyl alcohol gels. The water and hydrogel materials provide a soft medium biologically and biochemically compatible with addition of organic molecules, and are optimal for scientific laboratory studies. Polyester, polyurethane, and silicone phantoms are essentially permanent matrix suitable for routine calibration and testing of established systems.

The development of optical imaging techniques, like that of any other medical diagnostic modality, has relied upon appropriate phantoms whose physical properties and geometries are matched to those of human tissues. Measurements on phantoms are used to evaluate the performance of the systems and to validate imaging algorithms.

For testing imaging systems and algorithms in the laboratory, fluid-based phantoms are often the most appropriate. Fluids allow small solid targets of contrasting optical properties to be placed within them, and to be moved in and out to represent a regional change in blood volume and/or oxygenation. Most fluid phantom materials have been water-based, with appropriate absorption provided by inks, food coloring agents or industrial dyes.

The use of solid phantoms avoids these problems, and researchers have advocated various alternative recipes for generating them.

The main materials used for solid phantom are the silicon rubber, and polyvinyl alcohol (PVA) slime.

In our calibration experiments we have used 4 different fluid phantoms, namely: water, diluted solution 0.9 % NaCl, intralipid (lipofundin: 1 %, 10 % and 20 %), and diluted solution of bovine hemoglobin (Hb), and as solid barrier: glass recipients, latex thin film (from surgical gloves) or unique use recipients from PP (polypropylene) or PS (polystyrene).

3.1 Tissue simulating phantoms

Measurements of the transmittance of NIR light across tissue can be used to monitor changes in blood volume and its oxygenation. By making multiple measurements between pairs of points over the surface of a volume of tissue, it is possible to produce images which display the spatial variation in these physiological parameters. This is the basis of DOT, which is being widely explored as a means of generating functional maps in the adult female breast or to detect disease in the brain.

3.1.1 Fluid-based phantoms

For testing imaging systems and algorithms in the laboratory, fluid-based phantoms are often the most appropriate. A popular and inexpensive source of scattering for such phantoms has been intralipid, an intravenous nutrient consisting of an emulsion of phospholipids micelles and water. The optical properties of intralipid have been well characterized, and a 1 % intralipid concentration (of solid by volume) provides a medium with a transport scatter coefficient of roughly 1 mm^{-1} at NIR wavelengths.

A major disadvantage of fluid phantoms is that they require a barrier of solid material to contain the fluid and to separate regions of different optical properties. Other disadvantages are that they are often unstable over a prolonged period, and they are difficult to transport.

3.1.2 Solid phantoms

The optical properties of tissue have been simulated using RTV rubber, silicon sealant, colouring pigment in paraffin wax, ink and intralipid in agar, hemoglobin and intralipid in gelatin, cosmetic powder and aluminum oxide particles in silicon rubber, dye and titanium dioxide particles in polyester resin, dye and quartz glass spheres in polyester resin, and dye and amorphous silica spheres in epoxy resin.

The most common three choices for scatters have been: lipid based emulsions, titanium or aluminum oxide powders, and polymer microspheres. The choice of absorbers varies widely from hemoglobin and cells for biological simulation, to molecular dyes and ink as less biological but more stable absorbers.

3.1.3 Tissue phantom recipes

The absorbers typically utilized in constructing liquid tissue phantoms are ink, Hb, HbO_2, H_2O and lipid. Except the ink spectrum, well established spectra of the absorbers are available in Oregon Medical Laser Center (OMLC) homepage (http://omlc.ogi.edu/spectra/).

The ideal phantom material would be homogeneous with easily controllable optical properties, would have a long lifetime, could effortlessly be formed into complex shapes, and would have a reproducible design that is straightforward to prepare.

The absorption coefficient at each light wavelength is related to these chromophore contributions as follows:

$$\mu_a(\lambda, r) = \sum_{l}^{L} \varepsilon_l(\lambda) C_l(r) \tag{4}$$

where $\varepsilon_l(\lambda)$ is the extinction coefficient, $\boldsymbol{C}_l(r)$ the concentration of the lth chromophore and L is the total number of chromophores. As it was shown in Fig. 1, in physiological case, major chromophores are oxygenated hemoglobin (HbO_2), deoxygenated hemoglobin (Hb), H_2O, and lipids. The extinction coefficients, ε_{Hb}, ε_{HbO2}, ε_{H2O}, ε_{lipid} depend only on wavelength, λ, and have the dimension of [cm^{-1}/M].

The concentrations of these chromophores C_{Hb}, C_{HbO2}, C_{H2O}, C_{lipid} are given in [μM]. The scattering constraint comes from the observation that scattering in tissue follows a simplified Mie scattering approximation [1].

In the multi-spectral approach, the chromophore concentrations and scattering properties are reconstructed directly in a single step using data at all wavelengths with spectral constraints (Eqs. (3) and (4)).

The spectra of Hb and HbO_2 presented in the OMLC homepage are shown in molar extinction coefficients, ε.

From Beer's Law, the one-dimensional distribution of excitantion light I(λ,z) from surface to given depth z is

$I(\lambda,z) = I_0(\lambda)e^{-c\,\mu a(\lambda)z}$ where $I(\lambda,z)$ is the intensity of light at the medium surface.

The optical density is given by $-Log_{10}[I(z)/I_0]$, equal with $c\varepsilon(z)$, and according to mathematic equation $2.303Log_{10}(x)=Ln(x)$, the absorbtion coefficient can be computed from the molar extinction coefficient with the relation:

$$\mu_a(\lambda) = 2.303c\,\varepsilon(\lambda) \tag{5}$$

where μ_a is in (cm^{-1}), ε is the molar extinction coefficient for the wavelength of interest, and c is the concentration . The O_2 capacity of normal blood is 200 mL O_2/L.

Intralipid is a fluid used for intravenous feeding of patients and in the biomedical optics community is used as a scattering medium for phantoms that mimic turbid tissues when conducting optical experiments. Intralipid™ (Kabivitrum Inc., California and Stockholm) is a brandname for an aqueous suspension of lipid droplets sterile and suitable for intravenous feeding of patients. There are other brands: Nutralipid™ (Pharmicia, Quebec), Liposyn™ (Abbot Labs, Montreal), Lipofundin® MCT/LC (Braun Melsungen AG), which should be similar in composition, available as intralipid-10 % and intralipid-20 % (10 % lipid indicates 10 g of lipid per 100 mL of suspension).

The constituents of intralipid-10 % in a 500 mL bottle:

Soybean oil	50.00 g	53.94 mL
Lecithin	6.00 g	5.82 mL
Glycerin	11.25 g	8.92 mL
Water	430.50 g	431.33 mL
Total	497.75 g	500.00 mL

Fig. 4. The constituents of 10 % lipofundin and 10 % intralipid emulsion in conformity with the producer specifications.

According to van Staveren's Mie theory approximation [4], μ'_s of 10 % intralipid is given for a specified wavelength, λ, by the equations:

$$\mu_s = 2.54 \times 10^9 \times \lambda^{-2.4} \tag{6}$$

$$g = 1.1 - 0.58 \times 10^{-3}\lambda \tag{7}$$

$$\mu'_s = \mu_s(1 - g) \tag{8}$$

where λ is in [nm] and μ_s and μ'_s are in [cm^{-1}].

There is sufficient bottle-to-bottle variation in the optical properties of commercially available intralipid or other brandname products. Therefore the optical properties should be verified experimentally for each bottle at the time of use.

3.1.4 Calculation of intralipid concentration for a desired scattering

The intralipid is comercially available as 10 %, 20 % or 30 % solutions. In our case, we have used a 10 % lipofundin 500 mL bottle to prepare liquid lipofundin fantoms of 100 mL volume with different reduced scattering coefficients, μ'_s. For example, we can compute the needed volume of lipofundin to obtain phantoms with a reduced scattering coefficient of 1.02 mm^{-1} and 0.8 mm^{-1}, respectively. Using the equation (8), the absorption coefficient, μ'_s of the 10 % lipofundin can be obtained as 10.2 mm^{-1}. The needed volume of 10 % lipofundin solution can be calculated with:

$$\mu_s^{'before} \times V_{before} + \mu_s^{'\mathrm{int}\,ralipid} \times V^{\mathrm{int}\,ralipid} = \mu_s^{'after} \times V^{after} \tag{9}$$

and

$$\mu_s^{'k*10\%Intralipid} = k\mu_s^{'10\%Intralipid} \quad (10)$$

So, for a dilution 1:10 of 10 % lipofundin we obtain 1 % lipofundin and, consequently, the reduced scattering coefficient will be:

$$\mu_s^{'0.1\%Intralipid} = 0.1\times \mu_s^{'10\%Intralipid} = 1.02mm^{-1} \quad (11)$$

From the equation (10) we have:

$$0\times\left(100 - V^{10\%Intralipid}\right) + 10.2\times V^{10\%Intralipid} = 0.8\times 100 \quad (12)$$

$$V^{10\%Intralipid} = 7.84 \text{ mL.} \quad (13)$$

To control the absorption coefficient, μ_a, of liquid phantom we can add India ink in the intralipid solution. India ink is typically utilized for its monotonical spectra that makes it easy to produce expected absorption when testing μ_a response of the instrument at one wavelength.

If the measured absorbance is $Ab(\lambda)$, then

$$\mu_a(\lambda) = \ln(10)\times Ab(\lambda) = 2.3025 Ab(\lambda) \quad (14)$$

4. System calibration

The initial considerations used in the calibration of the diffuse optical tomography are: all source intensities and detector efficiencies are time invariant; each detector reading is a measure of light that has entered a target medium at only a single location (i.e., the light which is detected has exited from only a single location).

It is convenient to divide the calibration problem into three components: factors associated with the source fiber, the target medium, and with the detecting fiber [15].

If we note the fraction of light entering the target at the nth source fiber position with $I_{s,n}$ and the power of the laser diode with P_l, the overall source coupling efficiency coefficient, whose value varies for each optical path, will be:

$$s_n = \frac{I_{s,n}}{P_l} \quad (15)$$

Similarly to the equation (15), the overall detector coupling efficiency will be:

$$d_{n,j} = \frac{I_{t,j}}{I_{d,j}} \quad (16)$$

where $I_{t,j}$ is the light that exits the tissue at receiving fiber position, j, and $I_{d,j}$ the intensity of the light ultimately entering the detector.

If we consider the influence of the target medium on light propagation through the system expressed by m_{nj}, which is the fraction of photons launched into the target at location n, traveling through the medium, exits at location j, the transfer function of the entire measurement scheme will be [15]:

$$T_{nj} = s_n d_j m_{nj} P_l \quad (17)$$

where T_{nj} represents the power read by the detector acquired from the jth detector position with respect to the nth source position. In an experiment, the $i \times j$ detector readings are described by the expression $r_{nj} = cI_{nj}$, where c is the detector sensitivity, assumed to be constant. Using these last two relations, the transfer function can be expressed as a matrix equation:

$$R = c\, P_l SMD \quad (18)$$

where the elements in R are the detector readings, r_{nj}; S and D are diagonal matrices whose elements represent the composite loss factors, d_j and s_n, respectively; the elements in matrix M are the m_{nj} values attributable to losses occurring in the medium. The goal of calibration is to determine the entries of D and S, given the set of measured values in R.

The first step in the DOT calibration is the evaluation of the light transfer coefficients through optical fibers used as illumination sources and light receivers on the measuring head.

For precise measurement of the power in the input and the output of the optic fibres used for illuminations and detections we have used a laser radiometer Vega (Ophyr) equipped with a integrating sphere model 3A-IS-IRG as measuring head which has a resolution of 1 nW for a maximum power of 1 W, calibrated with 1 nm step in the NIR range.

The deviation from the maximum value is under 10 % and proceeds from the surface quality at the input and output of each optical fiber, from the dispersion of losses and the mechanical stress of each fiber in the measuring head, in the serial approach of the optical multiplexing.

The elements, r_{nj}, of the matrix, R, are the light intensity values used in the characterization of the optical properties of the target media (tissue phantom). They can be find either directly from the transfer equation using the iterative proportional fitting (IPF) technique [16] or solving the forward problem for a finite-element model [17].

From this representation it is easy to observe the dependence of the scattering processes of the irradiation wavelength and the nature of the media used as tissue simulating phantoms.

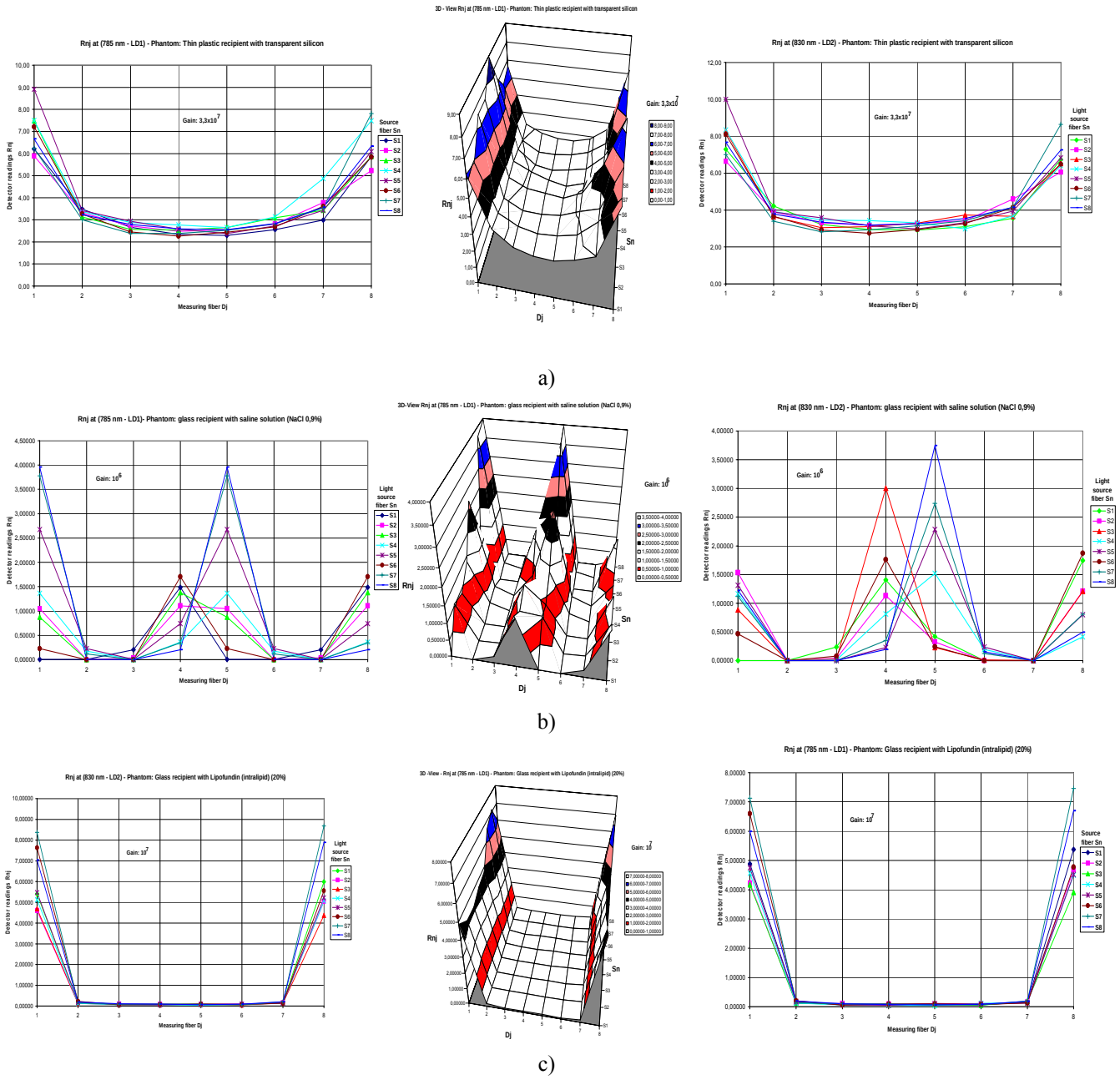

*Fig. 5. r_{nj} elements of the matrix R (detector readings) as a function of the detection fiber **j** and illumination fiber n for different tissue simulating phantoms: a) 1 % lipofundin, b) 10 % lipofundin, c) 0.9 % NaCl sterile solutions*

5. Modeling and reconstruction (forward and inverse problems

The image reconstruction problem in optical tomography is to estimate the optical properties within the object when the amount of guided light and the measured data on the boundary of the object are given. Image reconstruction problem in DOT is a non-linear ill-posed inverse problem.

The iterative solution of this problem requires repetitive solutions of the forward problem. Therefore, it is essential to have a computationally feasible forward model that accurately describes light propagation in the medium.

The forward problem in optical tomography is to solve the measurable data when the optical properties of the medium and the input light sources are given.

Light propagation in biological material is usually described by transport theory.

In transport theory, the most often applied forward models to describe light propagation in tissues are the radiative transfer equation and the diffusion approximation.

In the inverse problem of DOT, absorption and scattering functions, or in some studies absorption and diffusion functions, within the object are reconstructed. If more than one wavelength of light is used, the Hb concentration, oxygen saturation, and water distributions

can be calculated from the absorption spectra and some scattering characteristics from the scattering spectra [18]. Recently, there have also been studies in which the Hb, HbO_2, water, scatter amplitude, and scatter power have been directly estimated from the measurements at many wavelengths [1]. In this study, the reconstruction of the absorption and scattering coefficients $(\mu_a; \mu_s)$, or absorption and reduced scattering coefficients $(\mu_a; \mu'_s)$, are discussed.

6. Reconstruction of 2D absorption and scattering images

Let consider a cylindrical or spherical domain with circular boundary of diameter, D.

The medium is assumed to be homogeneous and isotropic, i.e., the absorption and scattering coefficients are assumed to be constant within the medium and the scattering probability is assumed to depend only on the angle between incoming and outgoing directions.

Furthermore, let n sources and j detectors be placed on circular symmetrical positions on the boundary of the domain. It should be noted that the number of the sources and the number of detectors does not need to be identical. However, that assumption is used here in order to simplify the computations.

Let us first assume that all sources and detectors are ideal in the sense that no amplitude losses or phase delays occur in the source and detector fibres.

Our experimental setup is an automated multi-channel frequency-domain system that use an overlaid intensity-modulated light from two laser diode (785 nm - 50 mW and 830 nm - 30 mW) sequentially sent to the phantom by eight 3-mm fiber optic bundles. For each source position, the diffused light is received at 8 detector positions along the surface of the cylindrical phantom. The serial approach for illuminations and detection is realized with one optical demultiplexer and one optical multiplexer. For each experimental configuration, a total of 128 measurements are performed in 1 minute.

For 2D reconstruction of the absorption and scattering images of the target media we have used a 50 mm diameter cylindrical liquid phantom (1 % lipofundin in a glass recipient) as the background medium, making the absorption coefficient, $\mu_a = 0.005$ mm^{-1} and the reduced scattering coefficient, μ'_s =1.0 mm^{-1}. A 14 mm diameter cylindrical solid object (polyamide bar) was embedded in the center of the background medium. Two cases with different optical contrast between the object and background were tested. The object in the first case was just an absorber with $\mu_a = 0.025$ mm^{-1} and $\mu'_s = 1.0$ mm^{-1}. Both μ_a and μ_s' for the object in the second case were different from the background: $\mu_a = 0.025$ mm^{-1} and $\mu'_s = 3.0$ mm^{-1}. The 2D finite-element mesh used had 3,341 nodes and 16,128 tetrahedral elements for both forward and inverse solutions.

The images presented in Fig. 10 were the results of 5 iterations with about 2 hours per iteration for reconstructing μ_a only (μ'_s of the object has been assumed known in the reconstruction for the pure absorber case) and 5 hours per iteration for reconstructing both μ_a and μ'_s in a PC with a Quad Core processor.

The image of the XY distribution of the μ_a and μ'_s is presented in figure 6. The reconstruction image of the phantom structure is in good agreement with the known geometry of the probe.

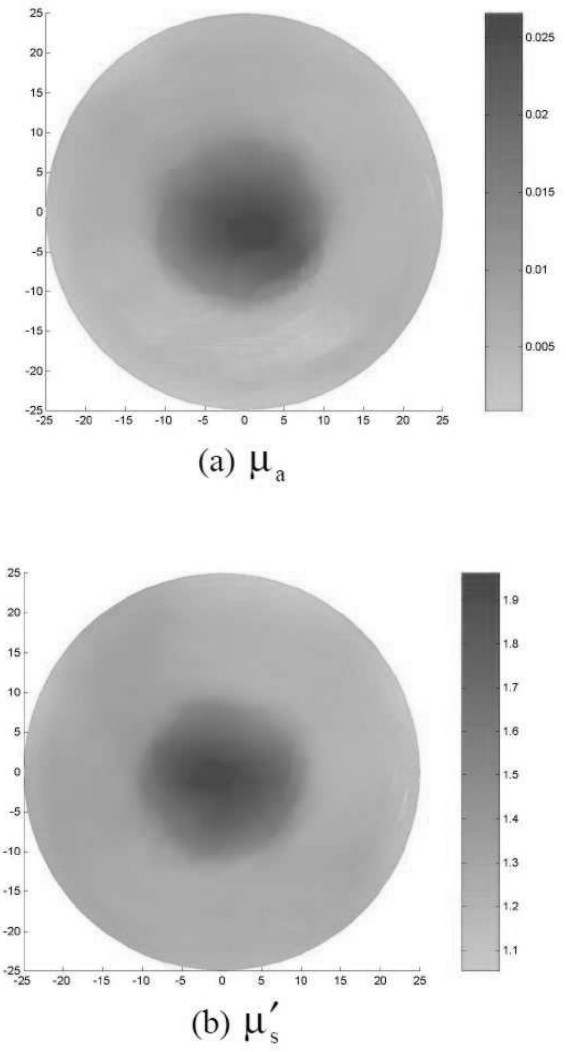

Fig. 6. The XY distribution of the absorption and reduced scattering coefficient for an intralipid 1 % solution with a central opaque bar inhomogeneity.

7. Conclusions

In order to obtain a high precision in the CW Diffuse Optical Tomography of turbid media the best way is to increase the number of the measuring data by enlarging the number of the wavelengths used to illuminate the target or to increase the number of the illuminating and measuring fibres.

The image high resolution needs the development of computation algorithms able to eliminate the influence of wall barriers and those of the imperfect contact between

the optical fibers and tissue. The use of thin latex membrane at the measuring boundary of the probe avoids the strong reflections and diffusion at the walls of the recipient.

The CW topology however needs a special effort to solve the non-uniqueness problem of the method which lacks the capability to separate absorption from scattering in the optical tomography image reconstruction. For this reason, the CW imaging needs preconditioning and regularization techniques and multispectral laser sources. The radiation used in ODP is non-ionizing and therefore this technique is safe for patients.

The technique developed as part of this research may also aid the development of new industrial applications where imaging through strongly scattering media is required, the measurement procedure.

References

[1] J. R. Mourant, T. Fuselier, J. Boyer, T. M. Johnson, I. J. Bigio, Appl. Opt. **39**, 949 (1997).

[2] X. Wang, B.W. Pogue, S. Jiang, H. Dehghani, X. Song, S. Srinivasan, B.A. Brooksby, K. D. Paulsen, C. Kogel. S.P. Poplack, W.A. Wells, J. of Biomed. Opt. **11**(4), 041106 /1–13 (2006).

[3] M. K. Nilsson, C. Sturesson, D. L. Liu, S. Andersson-Engels. Appl.Opt. **37**(7), 1256 (1998).

[4] H. J. van Staveren, C. J. M. Moes, J. van Marle, S. A. Prahl, M. J. C. van Gemert, Appl. Opt. **30,** 4507 (1991)

[5] D. A. Boas., Diffuse photon probes of structural and dynamical properties of turbid media: Theory and biomedical applications. Ph.D. dissertation University of Pennsylvania (1996).

[6] R. A. J. Groenhuis, H. A. Ferwerda, J. J. Ten Bosch., Appl. Opt. **22**, 2456 (1983).

[7] M. S. Patterson, J. D. Moulton, B. C.Wilson, K.W. Berndt, J. R. Lakowicz. Appl. Opt. **30**(31), 4474 (1991).

[8] S. A. Walker, S. Fantini, E. Gratton. Appl. Opt. **36**(1), 170 (1997).

[9] S. R. Arridge, P. van der Zee, M. Cope, D. T. Delpy, Proc. SPIE **1431**, 204 (1991).

[10] Christoph H. Schmitz, Mario Löcker, Joseph M. Lasker, Andreas H. Hielscher, Randall L. Barbour Rev. Sci. Instrum. **73**, 429 (2002)

[11] J. R. Mourant, T. Fuselier, J. Boyer, T. M. Johnson, I. J. Bigio, Appl. Opt. **39**, 949 (1997).

[12] Y. Xu, X. Gu, T. Khan, H. Jiang. Appl. Opt. **41**, 5427 (2002).

[13] M.K. Moaveni, A Multiple Scattering Field Theory Applied to Whole Blood, Ph.D. dissertation, Dept. of Electrical Engineering, University of Washington, 1970.

[14] S. Takatani, M. D. Graham, IEEE Trans. Biomed. Eng., BME-**26**, 656 (1987).

[15] Christoph H. Schmitz, Harry L.Graber, Hengbin Luo, Imran Arif, Jai Hira, Yaling Pei, Avraham Bluestone, Sheng Zhong, Randy Andronica, Ira Soller, Nestor Ramirez, San-Lian S. Barbour, Randall L. Barbour, Applied Optics **39**, 6466 (2000).

[16] J. Ripoll, V. Ntziachristos. Iterative boundary method for diffuse optical tomography. J. Opt. Soc. Am. A **20**(6), 1103 (2003).

[17] C.L. Matson, H.L. Liu, J. Opt. Soc. Am A **16,** 455 (1999).

[18] S. Srinivasan, B. W. Pogue, S. D. Jiang, H. Dehghani, C. Kogel, S. Soho, J. J. Gibson, T. D. Tosteson, S. P. Poplack, K. D. Paulsen. Proc. Natl. Acad. Sci. U. S. A. **100**, 12349 (2003).

[19] B. W. Pogue, S. D. Poplack, T. O. McBride, S. Jiang, U. L. Osterberg, K. D. Paulsen. Breast tissue and tumour haemoglobin and oxygen saturation imaging with multi-spectral near infrared computed tomography. In Adv. Exp. Med. Biol. International Society on Oxygen Transport to Tissue Plenum Press Aug. (2001).

[20] H.Wang, M. E. Putt, M. J. Emanuele, D. B. Shin, E. Glatstein, A. G. Yodh, T. M. Busch. Cancer Res. **64**, 7553 (2004).

[21] R. Choe, A. Corlu, K. Lee, T. Durduran, S. D. Konecky, M. Grosicka-Koptyra, S. R. Arridge, B. J. Czerniecki, D. L. Fraker, A. DeMichele, B. Chance, M. A. Rosen, A. G. Yodh, Med. Phys. **32**(4), 1128 (2005).

[22] C. H. Schmitz, H. L.Graber, H. Luo, I. Arif, J. Hira, Y. Pei, A. Bluestone, S. Zhong, R. Andronica, I. Soller, N. Ramirez, S. Barbour, R. L. Barbour, Applied Optics **39**, 6466 (2000).

[23] Y. M. M. Bishop, S. E. Fienberg, P. W. Holland, Maximum likelihood estimates for complete tables, in Discrete Multivariate Analysis: Theory and Practice MIT, Cambridge, Mass., (1991), Chap. 3.

[24] H. B. Jiang, Y. Xu, N. Iftimia, Optics Express **7**, 204 (2000).

*Corresponding author: mihai.patachia@inflpr.ro